GEOPHYSICS, VOL. 80, NO. 2 (MARCH-APRIL 2015); P. Q15–Q26, 20 FIGS., 1 TABLE.
10.1190/GEO2014-0373.1

Improving imaging and repeatability on land using virtual source redatuming with shallow buried receivers

Dmitry Alexandrov[1], Andrey Bakulin[2], Roy Burnstad[3], and Boris Kashtan[1]

ABSTRACT

Time-lapse surface seismic monitoring typically suffers from different sources of nonrepeatability related to acquisition imperfections as well as due to complexity of the subsurface. Placing sources and receivers below the surface can improve seismic data repeatability. However, it is not always possible to bury a large number of sources, and therefore the next best option is monitoring with surface sources and buried sensors. We have discovered that redatuming of surface sources to the shallow buried receivers produced a reliable image of target reflectors despite the fact that receivers were placed in the near-field zone of the source. We redatumed data with the virtual source method using crosscorrelation of the measured wavefields. We found that redatuming also reduced nonrepeatability of seismic data associated with changes in acquisition geometry, variable source coupling, and daily/seasonal variations in the near surface. We developed these results with a synthetic case study using a realistic 1D elastic model with a free surface and acquisition geometry from an actual field experiment conducted in Saudi Arabia.

INTRODUCTION

Repeatability of time-lapse seismic data is the single most important factor influencing permanent reservoir monitoring. Onshore seismic monitoring can especially suffer from various sources of nonrepeatability. Nonrepeatability causes time delays and amplitude changes that are obscuring 4D reservoir changes. It may originate from the source and receiver side as well as from variations in near-surface conditions. Schissele et al. (2009) show that these issues can be effectively addressed by burial of the sources and receivers. Although it can be feasible to bury a large number of receivers and a small number of sources in case of simple near surface (Forgues et al., 2011), a complex subsurface may still require significant fold to obtain a reliable image. Berron et al. (2012) present a case study of acquisition with sources and receivers buried at a small depth and demonstrate that imaging in a desert environment with a karsted near surface can be particularly challenging.

An alternative approach to burying the sensors and vibrators is to redatum the surface sources to the buried receiver positions. The simplest way to accomplish this without any velocity model is by applying the virtual source method (Bakulin and Calvert, 2006). This method reduces the influence of the complex near surface above the receivers, and it also improves repeatability (Bakulin et al., 2007; Mehta et al., 2008). A recent experiment in one of the onshore fields of Saudi Arabia (Bakulin et al., 2012) showed promising results for improving the seismic image and repeatability with the virtual source method. The seismic data were acquired using a densely populated source array and shallow buried receivers placed at a 30-m depth. Previous studies did not analyze repeatability improvements due to virtual source redatuming for such a shallow burial of receivers. In this study, we evaluate the imaging and repeatability for shallow buried receivers using a realistic elastic 1D model with a free surface.

Redatuming can also be accomplished with other methods such as multidimensional deconvolution (Wapenaar et al, 2010), which may also remove the free-surface multiples. This technique requires adequate receiver spacing, and in case of sparse receiver sampling, the redatuming can suffer from spatial aliasing (Hunziker et al., 2012). As such, we leave a trial of this approach for future studies.

We use elastic finite-difference modeling and perform our analysis in two steps. First, we focus on imaging the deep target reflector and estimating the redatuming parameters that provide the best possible image. To improve the image, we apply up-down wavefield decomposition at the receivers using dual-sensor summation (Barr, 1997). In addition, having the downgoing wavefield separated, we perform a detailed analysis of how the source-side ghosts affect

Manuscript received by the Editor 11 August 2014; revised manuscript received 8 November 2014; published online 27 February 2015.
[1]Saint Petersburg State University, Saint Petersburg, Russia. E-mail: dalexl30@gmail.com; bmkashtan@gmail.com.
[2]Saudi Aramco, EXPEC ARC, Dhahran, Saudi Arabia. E-mail: andrey.bakulin@aramco.com.
[3]Aramco Research Center, Houston, Texas, USA. E-mail: roy.burnstad@aramcoservices.com.

redatuming. We then turn to monitoring and compute a repeat data set with 4D noise induced by different factors, such as variable source coupling, source position errors, and changes in the near surface. We process buried receiver data using conventional and redatuming workflows, and we evaluate the effect of redatuming on the repeatability of the final time-lapse images.

VELOCITY MODEL AND ACQUISITION DESIGN

To generate synthetic data, we use a 2D finite-difference code. Figure 1a depicts a horizontally layered velocity model, which is based on the acoustic logs from an onshore field in Saudi Arabia (Bakulin et al., 2012). The model consists of a large number of highly contrasting layers with a target reflector at approximately a 2000-m depth. The top 15 m of the model represents sand cover. The sand layer thickness in the field experiment varies from a few meters to several tens of meters. The acoustic log we use is from the area in which the sand layer is thick. In the field, this happens to be an area with bad data quality. In the modeling scenario, it also represents data with a poor signal-to-noise ratio (S/N). Receivers are buried at a 30-m depth below the surface with 30-m inline spacing. Inspired by a real experiment, we use a collocated vertical geophone and hydrophone to perform a dual-sensor summation during the preprocessing stage. The seismic wavefield is generated by a vertical force source with 50-Hz dominant frequency acting on the surface. This simulates the surface seismic vibrator used in the experiment. An inline source sampling of 7.5 m simulates the actual field acquisition geometry.

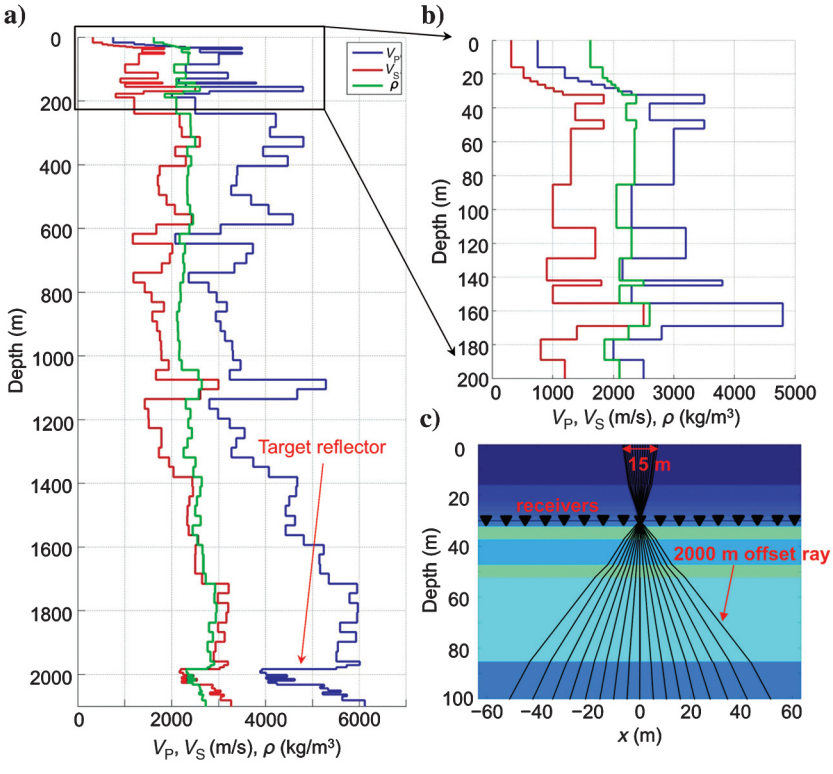

Figure 1. Realistic 1D elastic model used for the feasibility study. (a) P- and S-wave velocities and density from the surface to the target at 2 km, (b) a zoom of the near-surface portion, and (c) raypaths for reflections from the target horizon with offsets of up to 2000 m.

Due to rapid and monotonic increase of velocity within the topmost 30 m of the model (Figure 1b), raypaths experience strong bending in the near-surface part of the model. Ray tracing suggests that shooting a ray with only a 15° emergence angle away from the vertical direction will produce a 2-km offset for the deep reflection arrival (Figure 1c). Therefore, target reflections even at maximum offset of interest propagate mainly in the subvertical direction at the receiver level. This fact is important for the wavefield decomposition and will be used in the following section.

The free surface plays a significant role in the wavefield propagation. Full-waveform common-shot gathers for models without and with the free surface are substantially different (Figure 2). Here, we apply spherical divergence to compensate for geometric spreading for display purposes. In both models, numerous contrasting layers generate significant internal multiples. Analysis of synthetic vertical seismic profile (VSP) data with the methodology reported by Lesnikov and Owusu (2011) confirms this fact. In addition, slow surface waves and refracted arrivals obscure reflection events at large offsets. The presence of the free surface complicates the wavefield even more and leads to generation of free-surface multiples producing additional new low-velocity arrivals.

IMAGING WITH VIRTUAL SOURCE METHOD

Virtual source redatuming and a general workflow

The general workflow consists of three steps. During the first preprocessing step, we apply linear *f-k* filtering to remove strong surface waves and reveal reflection arrivals at larger offsets. Then, we perform virtual source redatuming. Finally, we apply NMO correction and stack the redatumed virtual source gather, which we refer to as a 1D stack. In this case, it represents a 1D image of our model.

To evaluate this 1D image, we compare it with two other stacks. The first one is the ground truth stack, which we obtain by NMO correcting and stacking of the buried source/buried receiver data with an actual source placed at a 30-m depth. Such a ground truth model assumes an elastic half-space above the 30-m level with the same elastic properties as the original model below. The second stack represents the VSP corridor stack (Lesnikov and Owusu, 2011). It contains only primary reflections without any multiples. At this stage, the goal is to develop an optimal workflow and determine those parameters for the virtual source redatuming that provide the best image of the target horizon at a 2-km depth and maximize the S/N.

The virtual source method is a redatuming technique that creates a virtual shot at the position of one of the receivers. This technique uses experimentally measured Green's functions from buried receivers and as such does not require knowledge of any velocity model (Bakulin and Calvert, 2006). The construction of the virtual source gather involves crosscorrelation of wavefields and stacking of crosscorrelations for each trace of the virtual source gather. The principal

part of the virtual source algorithm can be expressed in the frequency domain as a sum of the spectra products:

$$\hat{C}(x_B, x_A, \omega) = \sum_{S=1}^{N} \hat{u}(x_B, x_S, \omega)\hat{u}^*(x_A, x_S, \omega), \qquad (1)$$

where ω designates the angular frequency, $\hat{u}(x_B, x_S, \omega)$ is the spectrum of a signal generated by the source x_S and registered by receiver x_B, and $\hat{C}(x_B, x_A, \omega)$ is the spectrum of the virtual signal with receiver at x_B and the virtual source at x_A (Figure 3). Stacking is performed over either all sources x_S or some finite aperture of the sources. Here, the * symbol represents complex conjugation. Theoretically, this technique is valid for a generally heterogeneous lossless medium inside the volume bounded by the surface of integration. The assumption is made that the medium outside this volume is homogeneous (Wapenaar et al., 2010). This means, in particular, the absence of the free surface which can be a serious issue for surface seismic with free-surface multiples.

To illustrate the influence of the free surface, we start with a model without a free surface. Figure 4 shows the virtual source, ground truth, and VSP corridor stacks for this model. To plot these figures, we replicate the single-trace stack eight times to create a 1D image. We perform amplitude normalization with respect to the target arrival highlighted with a red line. The virtual source stack shows good agreement with the ground truth stack (Figure 4a). The VSP corridor stack contains only primary reflections and shows strong events at the same locations as the first two stacks. It also helps to appraise the number and strength of the internal multiples. They generate artificial reflections seen on the ground truth stack that are not observed on the VSP stack.

Results change significantly once we introduce a free surface into the model (Figure 4d). The free surface introduces additional noise and new multiples and noticeably complicates the wavefield. The target arrival (the signal) is still present on the virtual source stack, but the agreement with the ground truth stack is worse, and the amplitudes of other arrivals (noise) are significantly larger. Comparison between ground truth stacks for the models with and without the free surface shows the influence of the newly introduced free-surface multiples. Note that due to normalization, we keep the amplitude of the target arrival constant, so a decrease in the S/N effectively means an increase in the amplitudes of other arrivals on the stack. From now on, we will consider only the model with the free surface and aim to decrease the relative amplitude of these other arrivals.

Effect of the aperture size

The virtual source theory requires stacking over a closed surface populated with sources. In practice, stacking is usually performed over some finite area covered by the sources. The greatest contribution to the signal comes from the sources near the stationary phase point (Snieder et al., 2006), whereas sources further away enable destructive interference to reduce artifacts caused by summation of noncontributing parts of the crosscorrelations from an incomplete aperture (Bakulin and Calvert, 2006; Wapenaar, 2006). Figure 1c shows the ray-tracing results, which suggest that

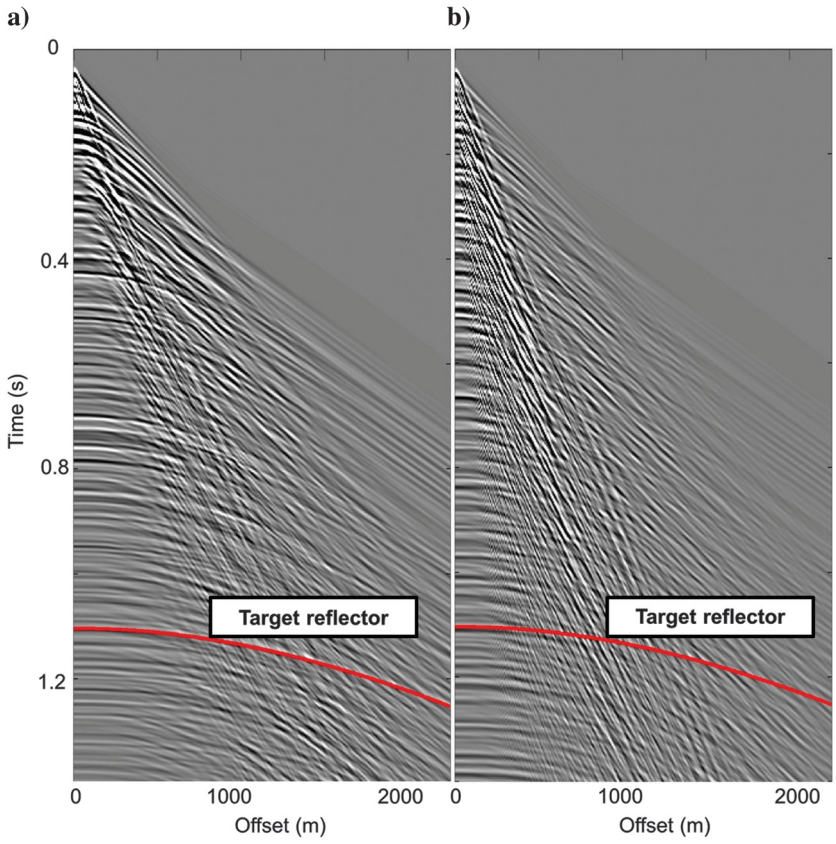

Figure 2. Common-shot gathers for the 1D model shown in Figure 1: (a) without the free surface and (b) with the free surface.

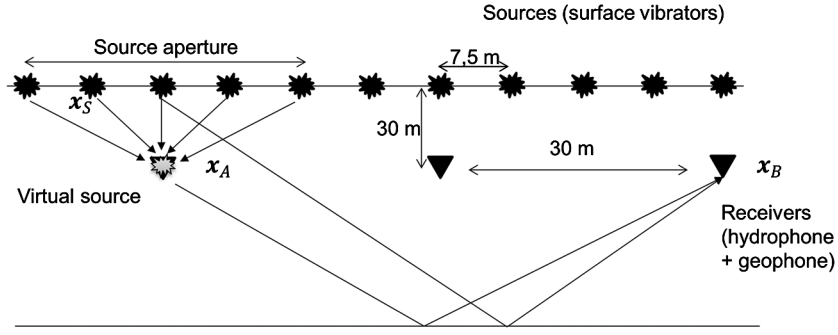

Figure 3. Idealized acquisition geometry.

an aperture of 15 m is enough to collect the main part of the energy into the virtual source. Due to a rapid increase of velocity in the near surface, rays departing at angles greater than 15° reach the critical angle before they arrive at the receiver level. Therefore, one may expect that the corresponding sources do not contribute to the virtual sources gather. However, ray theory assumes a high-frequency approximation of wave propagation, whereas for finite frequencies of interest, we do expect energy leaking and tunneling through relatively thin high-velocity layers (Cerveny and Aranha, 1992). Therefore, we will investigate source apertures that are significantly bigger than 15 m.

Figure 5 summarizes the results and suggest that redatuming with an aperture of 200 m produces the best virtual source image. This source aperture is significantly larger than that predicted by the ray theory. Values of the source aperture greater than 200 m do not change the resulting image. The amplitude of the target arrival is high-

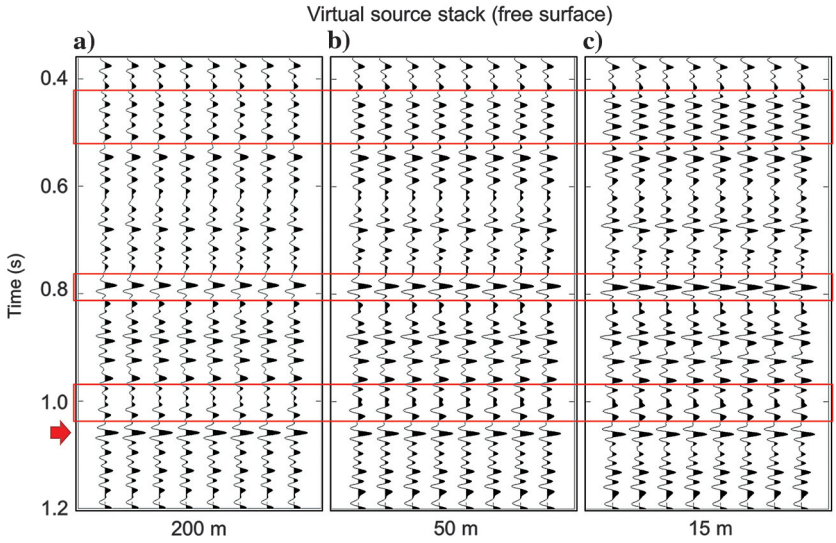

Figure 5. Virtual source 1D stacks obtained with a time gate length of 120 ms and different source aperture sizes: (a) 200, (b) 50, and (c) 15 m.

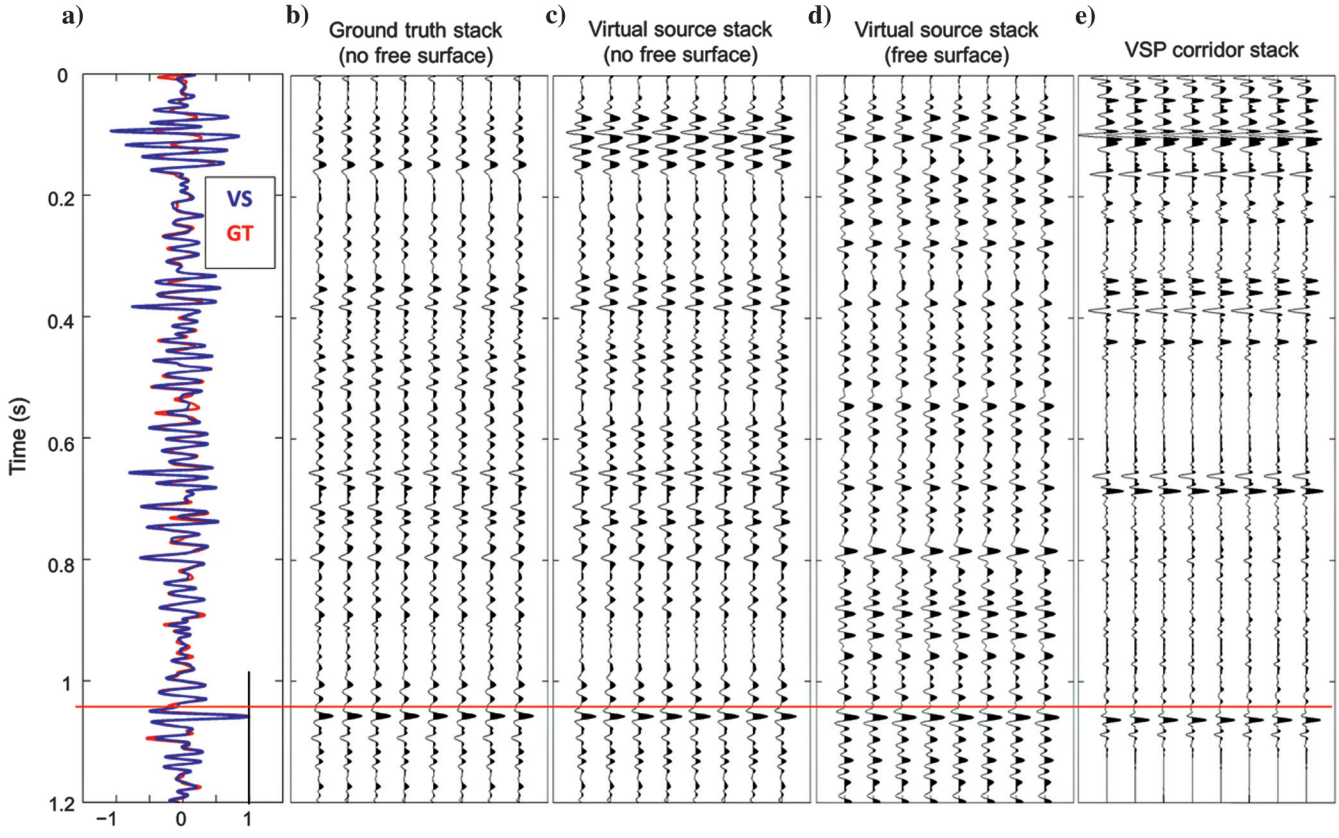

Figure 4. Comparison of 1D stacks including (a) overlaid virtual source stack (blue) for the model without a free surface and ground truth stack (red) traces for the model without a free surface obtained with actual buried sources at receiver locations, (b) the ground truth stack for the model without a free surface, (c) a virtual source stack for the model without a free surface, (d) the virtual source stack for the model with a free surface, and (e) a VSP corridor stack. Observe additional events related to internal multiples on panels (b and c) that are not present in panel (e). Likewise observe additional events related to surface multiples that are present in panel (d) but not in panel (c). The red line highlights the reflection from the reservoir.

lighted with the red arrow. Red frames indicate parts of the image that experience the biggest change with the source aperture variation. Decreasing the aperture to 50 or 15 m makes target reflections harder to identify: the highlighted unwanted events become stronger with respect to the target arrival.

Time gate selection

Bakulin and Calvert (2006) introduce the virtual source method and suggest using time gating before crosscorrelation in practice instead of crosscorrelating full wavefields. The time gating of the time-reversed wavefield around the first arrivals produces redatumed data with better S/N, and it helps to remove some spurious events related to an incomplete source aperture (van der Neut and Bakulin, 2008). In our model with shallow buried receivers, we find that increasing the time gate to include several events after the first arrival increases the amplitude of the target reflection. Figure 6 illustrates this fact and compares 1D virtual source stacks with time gates of different length. The time gate of 60-ms length includes direct arrival only. Using a twice-longer time gate increases the amplitude of the target reflection compared with the background events in the red frames. Increasing the time gate length further does not change the results significantly. We interpret these observations below.

Wavefield separation using dual-sensor summation

Mehta et al. (2007) demonstrate that up-down wavefield separation can significantly improve the quality of the virtual source image. Using the up- and downgoing wavefields instead of the full wavefield for crosscorrelation suppresses spurious events caused by free-surface multiples and an incomplete source aperture. Following the best practice for land, we compute prestack data for the geophone and hydrophone and combine them after noise removal to perform the wavefield separation. The geophone data set uses an adaptive scaling prior to summation. The rest of the processing steps, including the virtual source creation, follows the workflow described earlier. The virtual source images with wavefield separation introduce additional improvements. Figure 7 illustrates a significant increase of the S/N in images after up-down wavefield decomposition.

Dual-sensor summation delivers robust up-down decomposition in the case of near-vertical wave propagation at the receiver level. However, this method may fail at far offsets or for large propagation angles. As mentioned before, the ray-tracing analysis shows that reflected waves of interest at the receiver depth propagate in a subvertical direction (Figure 1c) and as such represents a favorable case for applying dual-sensor summation.

Why longer time gates may help

Having introduced the wavefield separation, we can illustrate why longer time gates help to improve the S/N. For this purpose, we analyze the downgoing wavefield in more details. Figure 8a shows the downgoing wavefield gated to the first 300 ms, which is not contaminated by any of the upgoing waves. Using ray tracing, we can identify several arrivals. The strongest events apart from the direct arrival can be classified as shallow and deep ghosts. Figure 9 shows a sketch illustrating propagation path of these arrivals. Shallow ghosts consist of the waves that reverberate in the topmost part of the model above the receiver level. Waves of this type reflect from shallow interfaces right below the sand layer, go up and bounce back from the free surface. Because the seismic wavelength is larger than the thickness of the topmost layers below the sand cover, the shallow ghost in Figure 8a is a superposition of waves reflected from several shallow horizons (Figure 9a) rather than from a single interface. The shallow ghost has a similar moveout to the direct arrival. The offset range of these waves is limited due to postcritical reflections occurring at larger offsets. However because of the energy leaking through thin near-surface layers, it is still greater than that suggested by the ray tracing (Figure 9a). Deep ghosts travel below the receiver line and reflect from

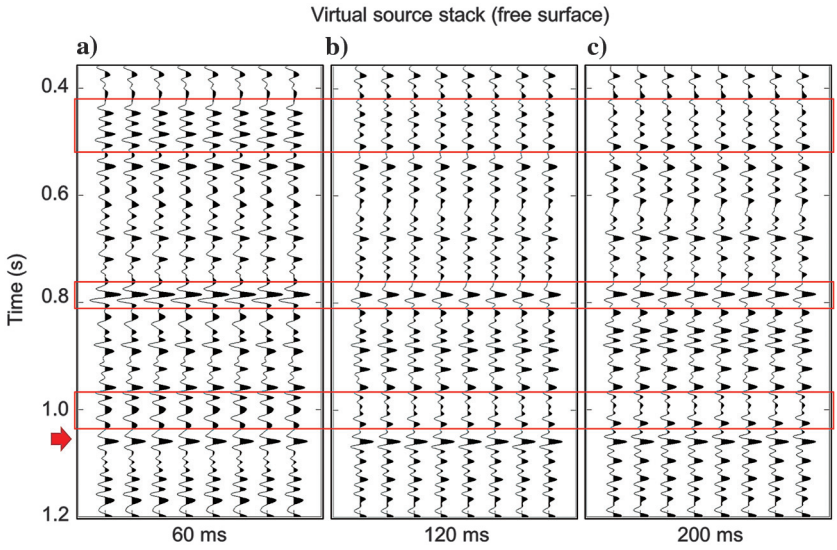

Figure 6. Virtual source 1D stacks obtained with a source aperture of 200 m and different time gate lengths: (a) 60, (b) 120, and (c) 200 ms.

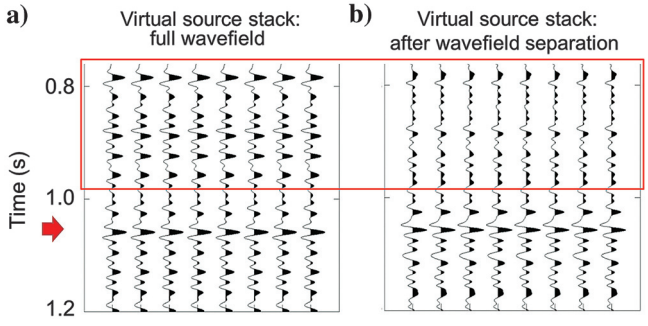

Figure 7. Magnifications of the virtual source 1D stacks after redatuming using (a) the full wavefield and (b) the decomposed wavefield. Note the reduction in the background reflectivity level above the target on panel (b), which makes it closer to the ground truth (Figure 4b) indicating that wavefield separation removes many spurious events associated with multiples.

one of the contrasting layers. Sensors register these waves after they have bounced from the free surface. These ghosts have weaker amplitudes, but they are visible over a larger range of offsets.

Both types of ghosts represent significant energy in the downgoing wavefield and contribute to the redatumed target reflections.

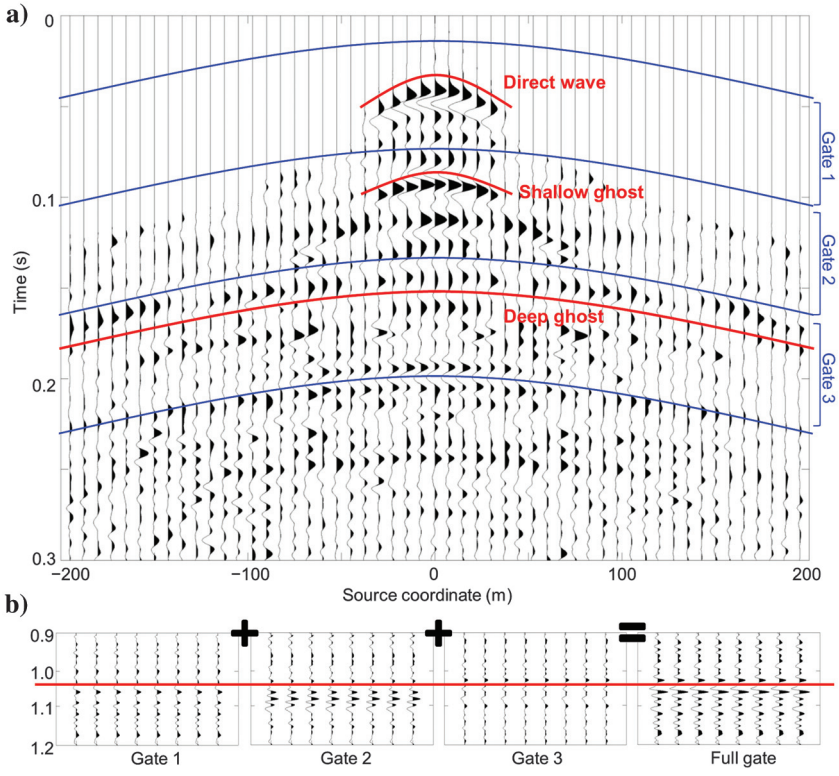

Figure 8. (a) The downgoing wavefield after production-type preprocessing. Different time gates used for crosscorrelation are shown by blue lines. (b) Magnifications of the virtual source 1D stacks obtained after redatuming with different time gates. "Full gate" is comprised of a combination of gates 1, 2, and 3 shown in panel (a). The red lines show some interpreted arrivals.

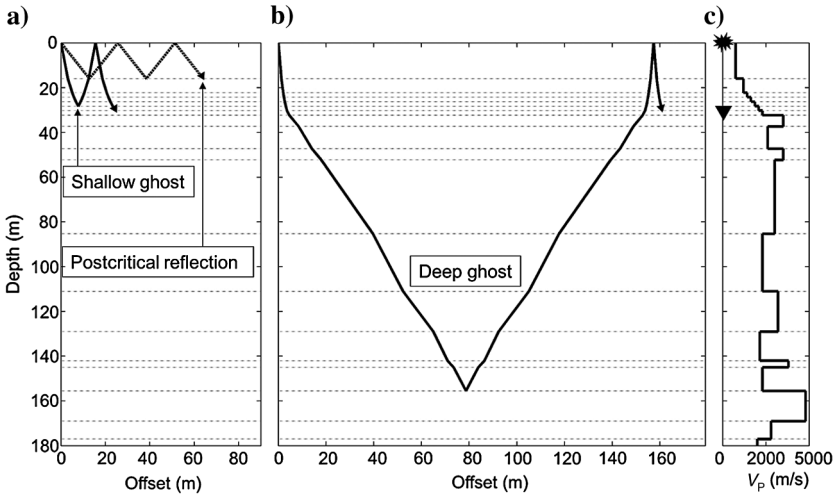

Figure 9. (a) Schematic path of downgoing shallow ghosts and (b) deep ghosts in the (c) near-surface part of the model.

Figure 10a and 10b shows two types of correlation gathers obtained by correlating upgoing ghost reflections at the receiver $x_B = 200$ m with the corresponding downgoing ghost arrivals at the receiver $x_A = 0$ m. The correlation gather represents individual trace-by-trace crosscorrelations or members of the sum of equation 1. All of these members will be summed to obtain a resulting virtual source trace. Because the distance from the receiver line to the target reflector is significantly larger than the source aperture used for summation, the reflection from this horizon will create an almost flat arrival on the seismogram for the selected offset range. As a result, moveouts on the correlation gathers resemble the moveouts of the downgoing ghost arrivals. The correlation gather in Figure 10c comprises crosscorrelations of the time-windowed downgoing field from Figure 8a with the upgoing field. After stacking, this gather will yield a virtual source trace with a 200-m offset. The direct wave and the shallow ghost events correlate with the upgoing field to produce strong steep events dominating the near offsets. In contrast, deeper ghosts produce events that are much weaker and flatter, but they are spread over a larger range of offsets.

To evaluate the contribution of the different types of ghosts to the target reflection on the virtual source gather, we split the time gate into three gates of equal length (Figure 8a). The first, shallow time gate contains the direct wave only, the second one includes the shallow and deep ghost energy, whereas the third one comprises only deep ghost arrivals. We then compute the virtual source stacks using each of these time gates, and we compare them with the stack obtained with the full time gate comprised of a combination of gates 1, 2, and 3 (Figure 8b). We normalize all traces so that the amplitude of the target arrival, indicated with the red line on the full gate stack, is equal to unity. The virtual source stack computed with the shallow time gate contains an event at the expected time for the reflection from the target horizon. However, the amplitude of this arrival is only slightly greater than the amplitudes of other events. Using the middle time gate in addition to the shallow one increases the signal amplitude, but it also introduces some artifacts right after the target event. The third time gate mainly reduces the artifacts and adds some minor energy to the signal. Using the full time gate of 180 ms length delivers the best result. This confirms that the direct arrival and deep and shallow source ghosts all contribute to the improvement of the S/N on the final virtual source image.

MONITORING WITH THE VIRTUAL SOURCE METHOD

Now that we demonstrate that the virtual source method can successfully perform redatuming of the shallow receiver data, let us turn

our attention to the repeatability of the redatumed images. To compare the repeatability achieved with and without redatuming, we follow the workflow displayed in Figure 11. We use the same finite-difference modeling but now compute baseline and monitor data. For the latter one, we introduce different kinds of 4D noise to simulate various nonrepeatabilities observed in the field. Note that the reservoir zone remains unchanged, so the actual 4D signal is zero. We subject baseline and monitor data to the same preprocessing steps, and we then process these data sets in two different ways:

1) conventionally by introducing vertical time shifts and stacking after NMO corrections
2) redatuming using the virtual source method and then stacking prestack virtual source data after NMO corrections.

We use the normalized root mean square (Nrms) error to quantify the differences between baseline and monitor stacks for virtual source and conventional processing. The Nrms is computed in a 150-ms section of the stacks centered around the target arrival at ~1.1 s two-way time. We repeat this workflow for each type of 4D noise to find out whether the source aperture size and time gate length can affect the repeatability of virtual source data.

Modeling land nonrepeatability

We consider three types of nonrepeatability causes for permanent land monitoring: acquisition geometry variations, source coupling variations, and seasonal changes of the elastic parameters of the near-surface layers. Inability of the vibrator to return to exactly the same location during repeated surveying leads to source geometry errors (Figure 12a). A previous experiment showed that even small changes in the vibrator position of less than 2 m can significantly reduce seismic data repeatability (Jervis et al., 2012). Although the effect on deep reflections may be small, at least in a 1D subsurface, the source position variation can strongly alter shot-generated noise propagating with low velocity of the near-surface layers (Figure 1a). Another serious issue that affects the surface source repeatability is the variation in the source coupling (Figure 12b). Even if the vibrator is returned to exactly the same location, the way that the vibrator baseplate interacts with the ground

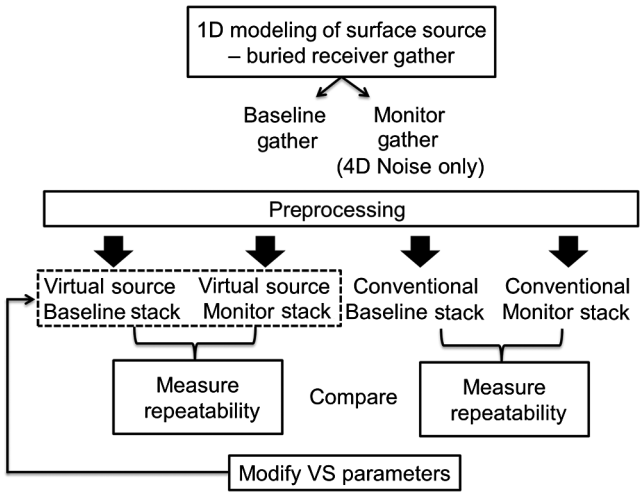

Figure 11. General workflow used for repeatability tests.

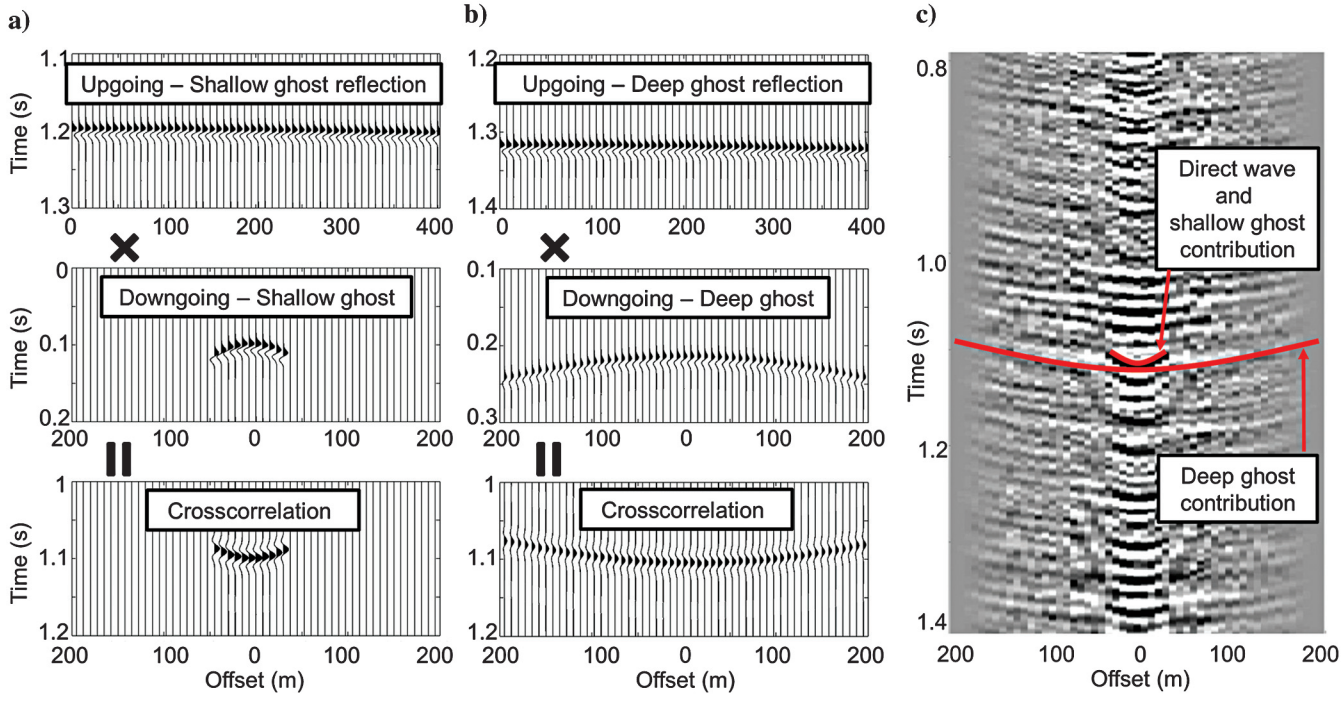

Figure 10. Correlation of the (a) shallow and (b) deep downgoing ghost arrivals with corresponding upgoing ghost reflections. After cross-correlation, both arrivals transform into the same primary reflection event. (c) The red lines indicate contributions of the direct wave, shallow, and deep ghosts to the virtual source correlation gather computed for an offset of 200 m.

can be different, especially in a desert environment with the sand surface changing the local topography over time. The compression of the soil under the vibrator plate can change the source wavelet as well. To model these types of source coupling changes, we apply arbitrary phase variations to each trace of the computed gather (Mehta et al., 2010). The amplitude spectrum of the source wavelet remains unmodified. Finally, daily and seasonal temperature and moisture variations may alter the elastic parameters of the surface layers and introduce 4D noise at the target level (Figure 12c). To simulate this effect, we modify the velocities in the first 2 m of the synthetic model.

Another issue that can degrade data repeatability in land monitoring is groundwater table variations. We do not consider this situation because in the experiment, the receivers were placed above the groundwater level and the water table depth remained constant throughout (Bakulin et al., 2014).

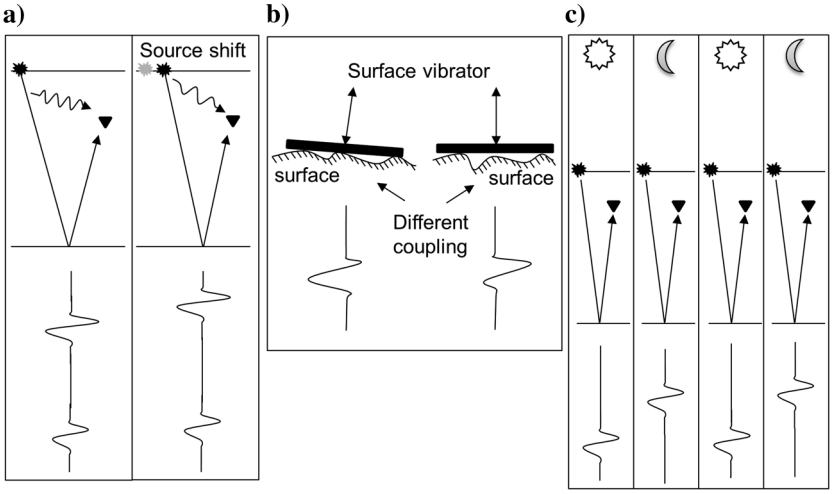

Figure 12. Cartoon depicting nonrepeatability causes identified for land 4D seismic with a surface vibrator: (a) acquisition geometry changes, (b) variable source coupling, and (c) daily/seasonal variations.

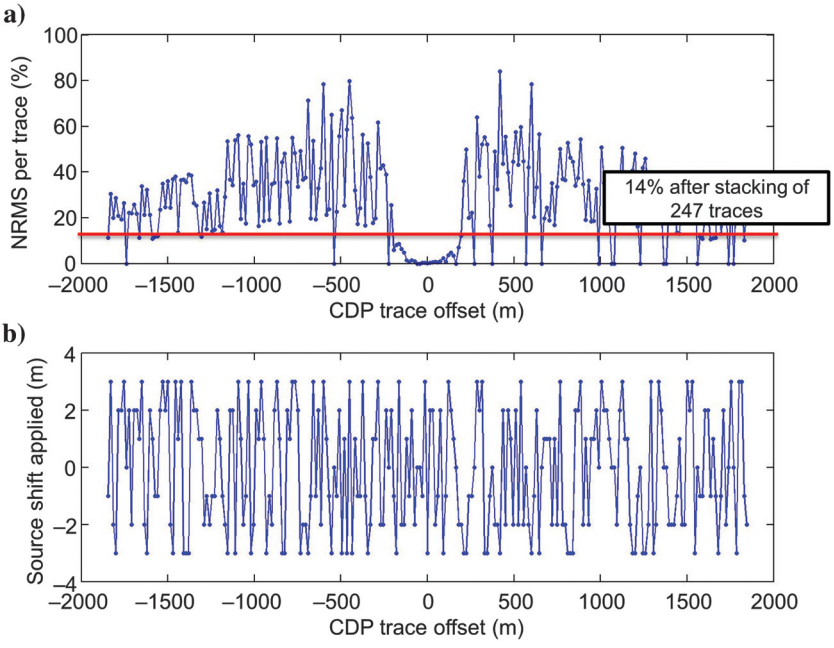

Figure 13. Nonrepeatability caused by variations in source positioning. (a) Nrms of prestack input traces and (b) actual source shift used for particular offset of the common depth point gather.

Geometry variations

To model geometry variations, we introduce random shifts of the source positions. Figure 13b shows the offset distribution of these shifts, which take integer values ranging from −3 to +3 m. We then compute the trace-by-trace Nrms between the baseline and the monitor gather in a window of 150-ms length around the target reflection (Figure 13a). No preprocessing is applied at this step. The Nrms at smaller offsets has low values of several percent, whereas at larger offsets, it can reach 60%–80%. We interpret this as a result of reflections obscured with surface waves at larger offsets. These horizontally propagating waves are much more sensitive to the source location variations than the deep reflections, but they start to dominate only at offsets of 200 m or greater.

Even without preprocessing, stacking across the offsets without redatuming gives an average Nrms value of 14%, if we use 247 traces (the red line in Figure 13a). If we apply *f-k* filtering and remove events with high wavenumbers, we reduce the average Nrms to 13.5%. If we additionally perform the up-down wavefield separation (using hydrophone and geophone summation) and stack the upgoing wavefield, we can achieve Nrms values of approximately 10% (Table 1).

Now, let us compare the repeatability of conventionally processed data with that obtained by virtual source redatuming. Figure 14 shows the Nrms for virtual source stacks obtained using correlation of (unseparated) geophone wavefields without preprocessing. We vary the aperture and time gate length in the same range as we did in the imaging section of the paper. Each column in the figure represents the Nrms for a pair of these parameters. The shortest time gate of 45 ms captures only the direct wave, whereas the gate with 180 ms also includes several source-side ghosts. Changing the aperture from 15 to 200 m corresponds to increasing the number of shot records used for correlation from 5 to 53. Note that although the conventional gather has 247 traces, the virtual source gather has only 83.

We observe improvements in repeatability for large values of the source aperture and gate size.

The Nrms drops to 8.5%. However, for a range of parameters, the Nrms goes above 12%. The 4D noise is transferred to the virtual source gather from the original data in several ways. The part of the wavefield that falls within the chosen time gate contains strong linear arrivals corresponding to surface and refracted waves (Figure 15a). A significant part of this kind of energy remains in the upper layers and propagates mainly in the horizontal direction. Being sensitive to the source position, these waves add nonrepeatable noise throughout the entire virtual source section after crosscorrelation. On the other hand, the same waves obscure reflections at large offsets, thus affecting both data sets used for correlation.

We can reduce the influence of refracted waves inside the gate by wavefield separation. Figure 15b confirms this and compares the downgoing wavefield relatively free of refracted waves with the full geophone wavefield. Indeed, the maximum Nrms of the virtual source gather constructed with correlation of the down- and upgoing wavefields does not exceed 10% as indicated in Figure 16a. Another way to improve repeatability is *f-k* filtering, which should effectively remove linear arrivals. Figure 16b confirms that *f-k* filtering brings the maximum Nrms for the selected range of parameters below 10% and gives the best value of 6.5%. To benefit from both methods and obtain optimal results, *f-k* filtering should follow up-down wavefield separation.

Variable coupling

To simulate variable coupling, we applied random phase shifts to each trace in the input gather. The average phase perturbation was 21°. Figure 17a shows an example of the phase variation for a single trace. After stacking the 247 input traces, the average Nrms error on conventional stacks reached 8.5% (red line in Figure 17b). Note that there is no obvious offset dependence of the per-trace Nrms because each trace has different phase shifts independent of the other traces.

We expect the virtual source redatuming to reduce this type of variation because the process of constructing the virtual source gather in the frequency domain includes multiplication of the spectra of one trace with the complex conjugate of another trace (equation 1). Both traces are recorded from the same phase-perturbed source. Therefore, phase variations should be canceled after the crosscorrelation. Numerical tests using the raw wavefield without *f-k* filtering confirm this (Figure 18a), resulting in average Nrms values for the virtual source stacks of less than 0.5%. However, applying linear *f-k* filtering before correlation of phase-shifted traces significantly alters the phase, and subsequent crosscorrelation does not completely remove phase variations. The average Nrms error increases up to 6% (Figure 18b), and only 2% incremental improvement is achieved compared with conventional 1D stacks.

Introducing simultaneous coupling and geometry variations in a shot gather yields 15% Nrms on stacks without redatuming. It can be reduced to 7% on the virtual source stacks by crosscorrelating the geophone wavefield only after the *f-k* filtering or by crosscorrelating the down- and upgoing wavefield without *f-k* filtering. In both cases, the Nrms error is reduced to almost the same level but

Table 1. Comparison of repeatability errors obtained with and without virtual source redatuming.

Nonrepeatability cause	Conventional stack	Virtual source stack	Preprocessing
Geometry variation	14.5%	8.5%	None
	10.2%	6%	*f-k* + wavefield separation
Coupling (modeled as phase variation)	8.5%	0.2%	None
	7%	0.2%	Wavefield separation
Geometry and coupling	15%	7%	*f-k*
Seasonal changes (top 2 m)	10%	5%	*f-k* + wavefield separation

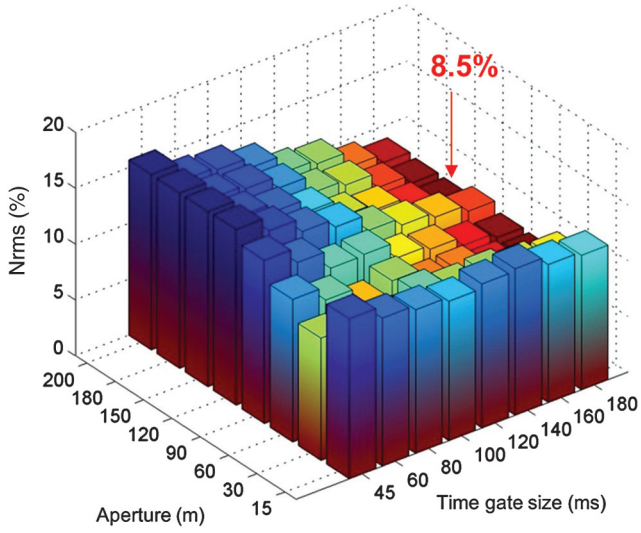

Figure 14. The Nrms due to geometry variations for virtual source stacks obtained using correlation of geophone data only.

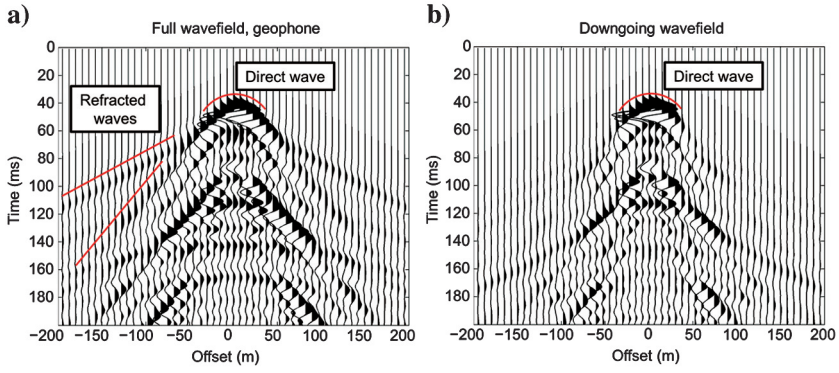

Figure 15. Seismograms showing (a) the full wavefield recorded by the geophone and (b) the downgoing field obtained after geophone and hydrophone summation.

for different reasons. The second approach almost perfectly eliminates coupling variations, but it is perhaps not as efficient at attacking the geometry changes. In contrast, the first approach is not as good at eliminating coupling variations, but it does a better job at correcting the geometry-induced nonrepeatability.

There can be other ways to model different source coupling. We considered only phase variations with constant amplitude spectrum. Because of the design, the virtual source method produces perfect results in this case. In case of more complex signal changes that affect the phase and amplitude spectrum, it can be preferable to remove the source signature from the seismogram before redatuming using deconvolution or perform redatuming with multidimensional deconvolution (Wapenaar et al., 2010).

Daily/seasonal variations

Daily and seasonal temperature variations can affect the elastic properties of the topmost layer of the near surface and lead to significant nonrepeatability (Schissele et al., 2009). To model this effect, we increase the elastic parameters within the first 2 m of the model by 1%. Figure 19 shows the prestack Nrms profile, computed between gathers for the base model and the model with modified parameters. Two symmetrical peaks of per-trace Nrms values clearly indicate the offset range at which surface waves dominate over the reflection arrivals. Similar to the case of geometry variations, surface waves are more sensitive to near-surface parameter variation. Without preprocessing, conventional stacks show 14.5% Nrms error, whereas wavefield separation and *f-k* filtering reduce this value to 10.2% (Table 1). To evaluate whether redatuming can reduce these effects as reported by Bakulin and Calvert (2006), we examine several scenarios: crosscorrelation of the full geophone wavefield (with or without *f-k* filtering) and crosscorrelation of the up- and downgoing wavefield (with and without *f-k* filtering). In all cases, the Nrms after redatuming decreased to 4%–5%. We note that generally larger values of the virtual source aperture produced lower Nrms values (Figure 20).

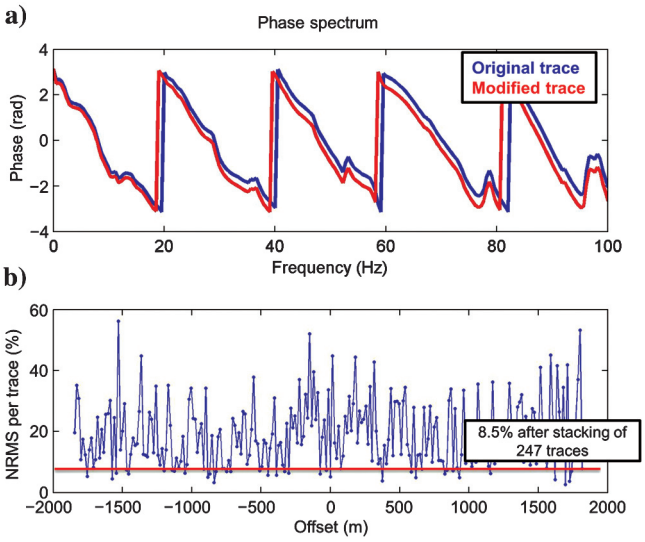

Figure 17. Simulating variable coupling of the seismic vibrator by phase perturbations: (a) phase spectra of a single trace with a 30-m offset before and after applying a phase perturbation and (b) Nrms errors for every trace of the input gather after applying phase variations.

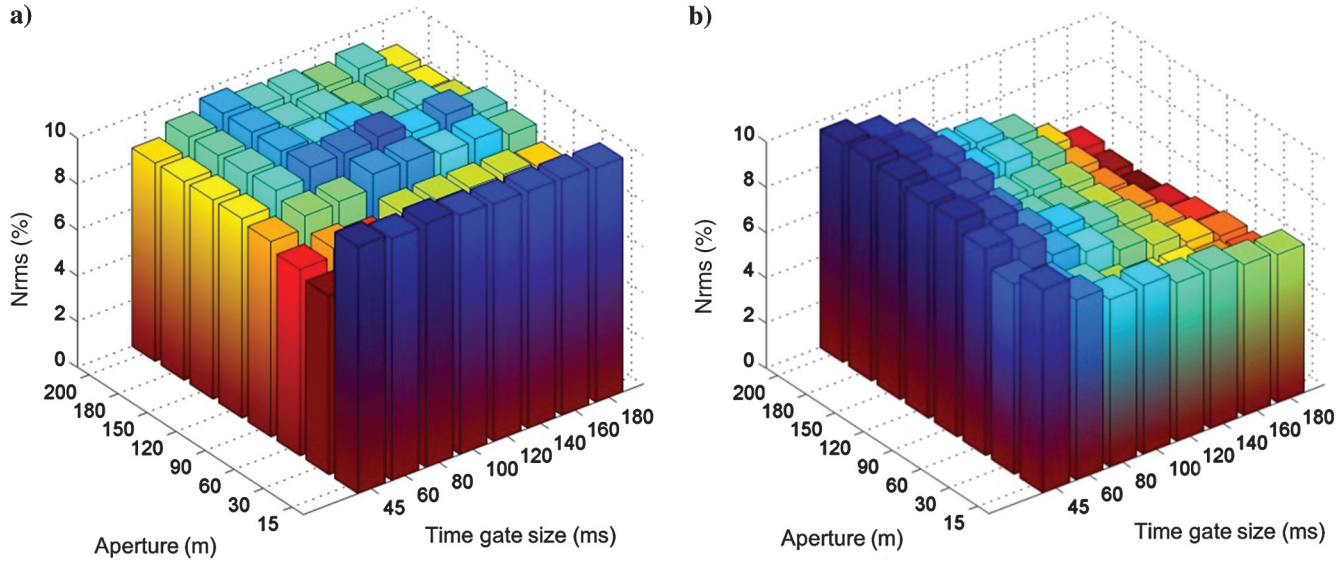

Figure 16. The Nrms error versus aperture and gate size for the virtual source stacks obtained after introducing geometry variations for two scenarios: (a) crosscorrelation of the down- and upgoing wavefield (without *f-k* filtering) and (b) crosscorrelation of the full geophone wavefield after linear filtering in the *f-k* domain.

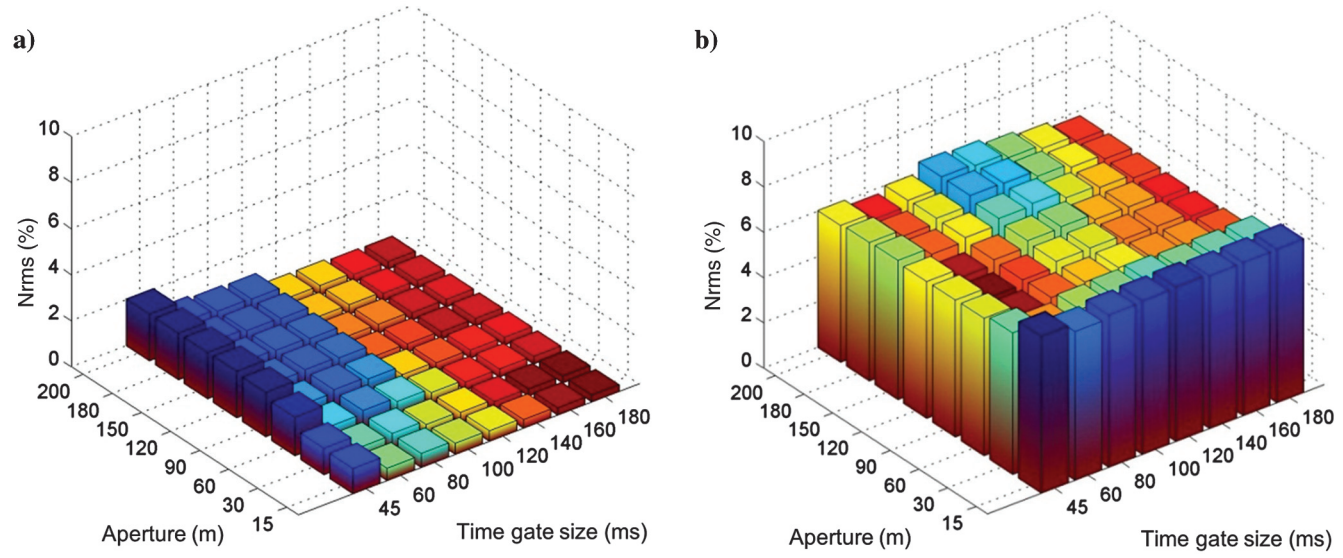

Figure 18. Nrms versus gate size and aperture for the virtual source stacks with variable coupling modeled as phase perturbations for the case of (a) crosscorrelation of the geophone recording only without preprocessing and (b) crosscorrelation of the geophone recording only after *f-k* filtering to suppress surface and refracted waves.

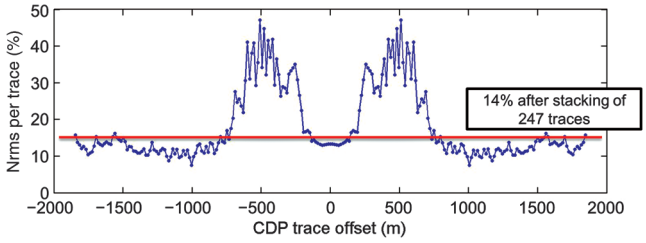

Figure 19. Nrms of prestack input traces caused by seasonal variation modeled as a 1% increase in P- and S-wave velocities and density of the topmost 2 m of the model.

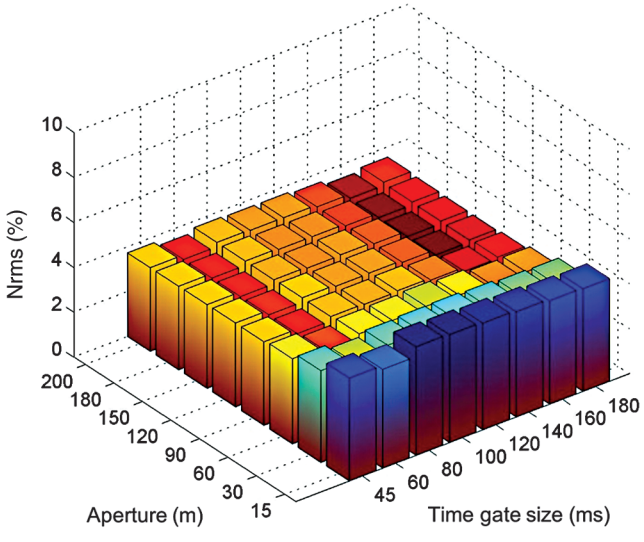

Figure 20. Nrms error versus aperture and gate size for virtual source stacks obtained after introducing seasonal variations for the case of crosscorrelation of the down- and upgoing wavefields with *f-k* filtering.

CONCLUSIONS

Using a synthetic case study, we demonstrated the feasibility of virtual source redatuming applied to seismic data acquired with shallow buried receivers. We have used a realistic elastic model with a free surface and as such included important land effects, such as surface waves, S-waves, and multiples. For the configuration at hand, the best virtual source images are obtained with a time gate of 180 ms and a source aperture of 200 m. These parameters provide the highest amplitude of the target reflection compared with other events on the virtual source stack. Applying up-down wavefield separation before crosscorrelation further improves redatumed images. Analysis of the downgoing wavefield showed the presence of the deep and shallow source-side ghosts, which positively contribute to the redatumed target arrival when included in the correlation process. This analysis led to optimal selection of a longer time gate and a larger source aperture size, which extend far beyond the window containing the direct wave only.

We also demonstrate that the virtual source method reduces nonrepeatability of seismic data caused by various types of 4D noise, such as geometry errors, different source couplings, and diurnal/seasonal variations of the elastic parameters of the topmost layers. We compare the poststack repeatability of the virtual source images with the conventional stacks and summarize the results in Table 1. The virtual source method proved to be most efficient in reducing nonrepeatability caused by variable source coupling modeled as phase perturbations in the source wavelet. Applying preprocessing before crosscorrelation to remove surface and refracted waves makes the results less impressive because trace mixing perturbs phase spectra and it lessens the efficiency of canceling these phase errors during correlation. On complex synthetic or real data, we have to perform noise removal before redatuming to suppress surface waves and other arrivals that are not handled during redatuming. Otherwise, the S/N will be low. For the data at hand, this is best done at the preprocessing stage when we can take full benefit from the dense source spacing of 7.5 m. Applying filtering after redatum-

ing to the redatumed virtual source gather can be problematic because the spacing is increased to 30 m. In contrast to source coupling nonrepeatability, we can remove 4D noise associated with source location errors as well as seasonal/moisture variations more effectively if *f-k* filtering is applied before redatuming. Another way to improve the repeatability is to use wavefield decomposition prior to correlation. Similar to the imaging case, a larger time gate and source aperture size proved to be more beneficial in improving repeatability confirming that there is no conflict between selecting the best parameters for the image and repeatability.

ACKNOWLEDGMENTS

We thank Saudi Aramco for support and permission to publish this work. This research was carried out using computational resources provided by the Resource Center Computer Center of Saint Petersburg State University (SPbU). The work was additionally supported by SPbU grant no. 11.38.217.2014.

REFERENCES

Bakulin, A., and R. Calvert, 2006, The virtual source method: Theory and case study: Geophysics, **71**, no. 4, SI139–SI150, doi: 10.1190/1.2216190.

Bakulin, A., M. Jervis, R. Burnstad, and P. Kelamis, 2012, The feasibility of permanent land seismic monitoring with buried geophones and hydrophones in a desert environment: 74th Annual International Conference and Exhibition, EAGE, Extended Abstracts, X039.

Bakulin, A., J. Lopez, A. Mateeva, and I. Sinha Herhold, 2007, Onshore monitoring with virtual-source seismic in horizontal wells: Challenges and solutions: 77th Annual International Meeting, SEG, Expanded Abstracts, 2893–2897.

Bakulin, A., R. Smith, M. Jervis, and R. Burnstad, 2014, Near surface changes and 4D seismic repeatability in desert environment: From days to years: 84th Annual International Meeting, SEG, Expanded Abstracts, 4843–4847.

Barr, F., 1997, Dual-sensor OBC technology: The Leading Edge, **16**, 45–52, doi: 10.1190/1.1437427.

Berron, C., E. Forgues, M. Jervis, A. Bakulin, and R. Burnstad, 2012, Buried sources and receivers in a Karsted desert environment: 74th Annual International Conference and Exhibition, EAGE, Extended Abstracts, X040.

Cerveny, V., and P. R. A. Aranha, 1992, Tunneling of seismic body waves through thin high-velocity layers in complex structures: Studia Geophysica et Geodaetica, **36**, 115–138, doi: 10.1007/BF01614124.

Forgues, E., E. Schisselé, and J. Cotton, 2011, Simultaneous active and passive seismic monitoring of steam-assisted heavy oil production: The Leading Edge, **30**, 1288–1294, doi: 10.1190/1.3663401.

Hunziker, J., E. Slob, Y. Fan, R. Snieder, and K. Wapenaar, 2012, Two-dimensional controlled-source electromagnetic interferometry by multidimensional deconvolution: Spatial sampling aspects: Geophysical Prospecting, **60**, 974–994, doi: 10.1111/j.1365-2478.2011.01019.x.

Jervis, M., A. Bakulin, R. Burnstad, C. Beron, and E. Forgues, 2012, Observations of surface vibrator repeatability in a desert environment: 74th Annual International Conference and Exhibition, EAGE, Extended Abstracts, X039.

Lesnikov, V., and J. Owusu, 2011, Understanding the mechanism of interbed multiple generation using VSP data: 81st Annual International Meeting, SEG, Expanded Abstracts, 4258–4262.

Mehta, K., A. Bakulin, J. Sheiman, R. Calvert, and R. Snieder, 2007, Improving the virtual source method by wavefield separation: Geophysics, **72**, no. 4, V79–V86, doi: 10.1190/1.2733020.

Mehta, K., J. Lopez, P. Matheny, and G. Rocco, 2010, Robustness of virtual source surveys in horizontal wells for reservoir monitoring in South Oman: 80th Annual International Meeting, SEG, Expanded Abstracts, 4185–4189.

Mehta, K., J. Sheiman, R. Snieder, and R. Calvert, 2008, Strengthening the virtual-source method for time-lapse monitoring: Geophysics, **73**, no. 3, S73–S80, doi: 10.1190/1.2894468.

Schissele, E., E. Forgues, J. Echappé, J. Meunier, O. de Pellegars, and C. Hubans, 2009, Seismic repeatability — Is there a limit?: 71st Annual International Conference & Exhibition, EAGE, Extended Abstracts, V021.

Snieder, R., K. Wapenaar, and K. Larner, 2006, Spurious multiples in seismic interferometry of primaries: Geophysics, **71**, no. 4, SI111–SI124, doi: 10.1190/1.2211507.

van der Neut, J., and A. Bakulin, 2008, The effects of time-gating and radiation correction on virtual source data: 78th Annual International Meeting, SEG, Expanded Abstracts, 2922–2926.

Wapenaar, K., 2006, Green's function retrieval by cross-correlation in case of one-sided illumination: Geophysical Research Letters, **33**, L19304, doi: 10.1029/2006GL027747.

Wapenaar, K., E. Slob, R. Snieder, and A. Curtis, 2010, Tutorial on seismic interferometry. Part 2: Underlying theory and new advances: Geophysics, **75**, no. 5, A211–A227, 10.1190/1.3463440.

Wapenaar, K., and J. van der Neut, 2010, A representation for Green's function retrieval by multidimensional deconvolution: Journal of the Acoustical Society of America, **128**, EL366–EL371, doi: 10.1121/1.3509797.